

Study on accelerator neutrino detection at a spallation source^{*}

Huang Ming-Yang^{1,2;1)}

¹ Institute of High Energy Physics (IHEP), Chinese Academy of Sciences (CAS), Beijing 100049, China

² Dongguan Institute of Neutron Science (DINS), Dongguan 523808, China

Abstract:

In this paper, we study the detection of accelerator neutrinos produced at the China Spallation Neutron Source (CSNS). Using the code FLUKA, we have simulated the production of neutrinos in the proton beam on the tungsten target and obtained the yield efficiency, numerical flux, and average energy of different flavors of neutrinos. Furthermore, detections of these accelerator neutrinos are investigated in two reaction channels, the neutrino-electron reactions and neutrino-carbon reactions. The event numbers of different flavors of neutrinos have also been calculated.

Key words: spallation source, accelerator neutrinos, numerical flux, event number

PACS: 14.60.Pq, 25.40.Sc, 29.25.-t

1 Introduction

In the past several decades, a number of spallation neutron sources have started to operate, such as the Los Alamos Meson Physics Facility (LAMPF), the Spallation Neutron Source at Rutherford Appleton Laboratory (ISIS) [1], the Japan Accelerator Research Complex (J-PARC) [2], the Spallation Neutron Source at Oak Ridge National Laboratory (SNS) [3], etc. In recent years, new spallation neutron sources are under construction, such as the China Spallation Neutron Source (CSNS)

[4], the European Spallation Neutron Source (ESS) [5], etc. These spallation neutron sources are designed to provide wide multidisciplinary platforms for scientific research and industrial applications at national institutes, universities, and industrial laboratories [6, 7]. The areas concerned include basic energy sciences, particle physics, and nuclear sciences. Table 1 shows the main technical parameters of several major spallation neutron sources at the GeV energy range. For J-PARC, the technical parameters shown in the table refer to the Rapid Cycling Synchrotron (RCS).

Table 1. Main technical parameters for several spallation neutron sources at the GeV energy range (ppp means protons per pulse).

	Extraction energy (GeV)	Extraction power (MW)	Repetition rate (Hz)	Average beam Current (mA)	Intensity (10^{13} ppp)	Target
LAMPF [8]	0.8	0.056	120	1	2.3	Various
ISIS [9, 10]	0.8	0.16	50	0.2	2.5	Water cooled /Tantalum
J-PARC [11, 12]	3.0	1.0	25	0.333	8.3	Mercury
SNS [13, 14]	1.0	1.4	60	1.6	16	Mercury
CSNS-I(II) [15, 16]	1.6	0.1(0.5)	25	0.063(0.315)	1.56(7.8)	Tungsten
ESS [17]	2.0	5.0	14	62.5	110	Tungsten

The CSNS consists of an 80 MeV proton linac, a 1.6 GeV RCS, a solid tungsten target station, and various instruments for applications spallation neutrons [18]. The accelerator operates at 25 Hz repetition rate with an initial design beam power of 100 kW and can be upgraded to 500 kW. As the exclusive spallation neutron source in developing countries, CSNS will be among the top four of such facilities in the world upon completion. Table 2 shows the main design parameters of CSNS-I and CSNS-

II [15, 16].

A large number of neutrinos can be produced at the beam stops of high intensity proton accelerators. They form the neutrino beams for basic scientific studies to better understand properties of neutrinos and better probes of the weak interaction force [19]. During the last several decades, many neutrino experiments have performed based on neutrino beams from spallation neutron sources [20] and other proton accelerators. They in-

* Supported by National Natural Science Foundation of China (Nos.11205185 and 11175020)

1) E-mail: huangmy@ihep.ac.cn

clude the Liquid Scintillator Neutrino Detector (LSND) [8] at LAMPF, the Karlsruhe Rutherford Medium Energy Neutrino experiment (KARMEN) [21, 22] at ISIS, the Tokai-to-Kamioka experiment (T2K) [23] at J-PARC and so on. For CSNS, similar to other accelerators, an intensive beam of accelerator neutrinos can be brought by the proton beam hitting on the tungsten target. By using a neutrino detector similar to MiniBooNE [24], different flavors of neutrinos can be detected. Therefore, neutrino properties, such as neutrino mixing parameters and the mass hierarchy may be studied.

Table 2. Main design parameters of CSNS.

Parameter/unit	CSNS-I	CSNS-II
Beam power on target/MW	0.1	0.5
Linac energy/GeV	0.08	0.25
Beam energy on target/GeV	1.6	1.6
Average beam current/ μA	62.5	315
Pulse repetition rate/Hz	25	25
Ion type, source linac	H^-	H^-
Protons per pulse/ 10^{13}	1.56	7.8
Target material	Tungsten	Tungsten
Target number	1	1
Target size/ mm^3	$50 \times 150 \times 400$	$50 \times 150 \times 400$
Beam section/ mm^2	40×100	40×100

2 Accelerator Neutrino Beam

The idea of using accelerator neutrino beam to study neutrinos was initiated independently by Schwartz and Pontecorvo, and the experiment was first carried out by Lederman, Schwartz, Steinberger and collaborators [19, 25]. Low energy neutrino beams can be produced by the decays of π and μ at rest, which are generated in low energy proton beams hitting on targets. In a beam dump experiment, the target for the primary proton beam, where the neutrino parent particles emerge, is the medium for absorbing or stopping the hadrons. Then no drift space is provided for hadrons to decay in. Therefore, high intensity and low energy proton accelerators ($p_{beam} \sim 1 \text{ GeV}/c$) such as spallation neutron sources are commonly used [26, 27]. The two recent experiments at a beam dump, LSND and KARMEN, have given controversial results on neutrino oscillations which have been resolved by the MiniBooNE experiment [28, 29].

The dominant decay scheme that produces neutrinos from a stopped pion source is [30]

$$\pi^+ \rightarrow \mu^+ + \nu_\mu, \quad \tau_\pi = 26\text{ns}, \quad (1)$$

followed by

$$\mu^+ \rightarrow e^+ + \bar{\nu}_\mu + \nu_e, \quad \tau_\mu = 2.2\mu\text{s}, \quad (2)$$

where $\tau_\pi(\tau_\mu)$ is the life time of $\pi^+(\mu^+)$.

The bulk of the π^- 's generated are strongly absorbed by the target before they are able to decay, and most of the μ^- 's produced from the π^- decay are captured from the atomic orbit, a process which does not give rise to $\bar{\nu}_e$. Therefore, the yield efficiency of $\bar{\nu}_e$ is a factor of 10^{-3} to 10^{-4} lower, and it will be neglected in the following discussions.

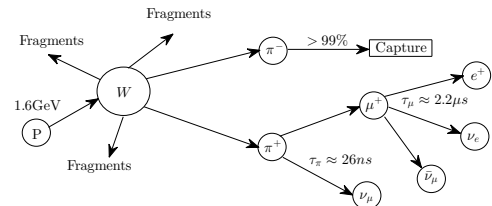


Fig. 1. The production mechanism of accelerator neutrinos at CSNS.

The CSNS beam stop will provide a copious flux of neutrinos, primarily from π^+ and μ^+ decays. Fig. 1 shows the scheme of neutrino production in the tungsten beam stop. By using the code FLUKA [31] and the main design parameters given in Table 2, the processes that the 1.6 GeV proton beam hitting the tungsten target were simulated. The results show that, after the complete decays of π^+ and μ^+ , three different species of neutrinos (ν_e , ν_μ , $\bar{\nu}_\mu$) produced have the same yield efficiency which is about 0.17 per proton. In Table 3, the event numbers per year of accelerator neutrinos produced at CSNS are given. We find that the three species of accelerator neutrinos have the same yield event number per year which is 0.21×10^{22} for CSNS-I and 1.05×10^{22} for CSNS-II. Since it will rise ultimately to 500 kW in the future with more neutrinos generated, the main parameters for CSNS-II will be considered mainly in the following research.

Table 3. Event numbers per year of accelerator neutrinos produced at CSNS.

	CSNS-I	CSNS-II
Proton number per year/ 10^{22}	1.23	6.15
ν_e number per year/ 10^{22}	0.21	1.05
ν_μ number per year/ 10^{22}	0.21	1.05
$\bar{\nu}_\mu$ number per year/ 10^{22}	0.21	1.05

The numerical flux ϕ of each particle (π^+ , μ^+ , ν_e , ν_μ , $\bar{\nu}_\mu$) can be found in [32]

$$\phi(L) = \frac{\varphi(\text{num/year})}{4\pi L^2(\text{cm}^2)}, \quad (3)$$

where L is the distance of the spallation target from the neutrino detector, and φ is the yield event number per

year. By using FLUKA, the yield efficiency of different particles can be obtained, then the numerical flux can be calculated using Eq. (3). Fig. 2 shows that:

- (i) Numerical fluxes of various particles involved decrease with the distance L ;
- (ii) ν_e and $\bar{\nu}_\mu$ have the same numerical flux;
- (iii) The numerical flux of ν_μ is larger than those of ν_e and $\bar{\nu}_\mu$;
- (iv) The numerical flux of π^+ decreases very quickly with the distance L .

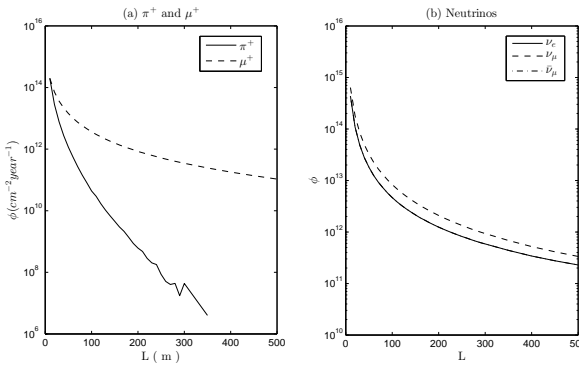


Fig. 2. The numerical flux of each particle (π^+ , μ^+ , ν_e , ν_μ , $\bar{\nu}_\mu$) as a function of the distance L . (a) π^+ and μ^+ ; (b) ν_e , ν_μ , and $\bar{\nu}_\mu$.

From the simulation results of neutrino productions, the average energy of different species of neutrinos can be obtained. The energy spectra of the different species of neutrinos are given in Fig. 3. It can be obtained that the average energy of ν_e is much smaller than that of ν_μ and $\bar{\nu}_\mu$.

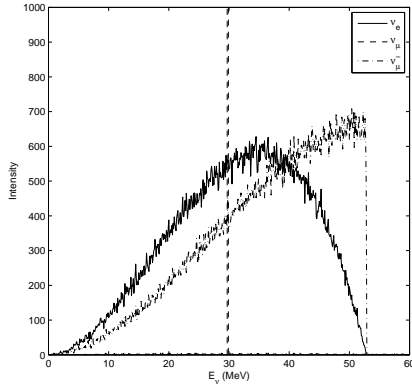


Fig. 3. Accelerator neutrino energy spectra at CSNS.

Because of the flavor mixing there are oscillations among ν_e , ν_μ , and ν_τ [33–35]. In the three flavor mixing scheme, neglecting the matter effect, and using the fact $\Delta m_{21}^2 = 7.5 \times 10^{-5} \text{ eV}^2$ and $L/E_\nu \simeq 1$, hence

$\sin^2(\Delta m_{21}^2 \cdot L / 4E_\nu) \simeq 0$, we can write the oscillation probabilities [36]

$$\begin{aligned} P(\nu_e \rightarrow \nu_\mu) &\simeq \sin^2 \theta_{23} \sin^2 2\theta_{13} \sin^2(\Delta m_{32}^2 \cdot L / 4E_\nu), \\ P(\nu_e \rightarrow \nu_\tau) &\simeq \cos^2 \theta_{23} \sin^2 2\theta_{13} \sin^2(\Delta m_{32}^2 \cdot L / 4E_\nu), \\ P(\nu_\mu \rightarrow \nu_\tau) &\simeq \cos^4 \theta_{13} \sin^2 2\theta_{23} \sin^2(\Delta m_{32}^2 \cdot L / 4E_\nu), \end{aligned} \quad (4)$$

where $|\Delta m_{32}^2| = 2.4 \times 10^{-3} \text{ eV}^2$, $\sin^2 \theta_{23} = 0.446$, $\sin^2 \theta_{13} = 0.0237$ [37], E_ν is the neutrino energy, and L is the distance of the neutrino source from the detector. Given the distance $L = 60$ m the simulation results show that the average energy of ν_e , ν_μ , and $\bar{\nu}_\mu$ are 33.0 MeV, 50.0 MeV, 47.9 MeV respectively. The oscillation probabilities can be calculated as $P(\nu_e \rightarrow \nu_\mu) \simeq 1.27 \times 10^{-6}$, $P(\nu_e \rightarrow \nu_\tau) \simeq 1.57 \times 10^{-6}$, and $P(\nu_\mu \rightarrow \nu_\tau) \simeq 1.26 \times 10^{-5}$. Therefore, due to the very short baseline, the oscillations among ν_e , ν_μ , and ν_τ can be neglected and will not enter our discussions below.

In the next section, processes of the accelerator neutrino detection will be studied, and the corresponding neutrino event numbers observed through various reaction channels will be calculated.

3 Detection of accelerator neutrinos

The event numbers per year \tilde{N}_i of accelerator neutrinos observed through various reaction channels i can be calculated following [38]

$$\tilde{N}_i = \phi(\nu/\text{year}/\text{cm}^2) \cdot \sigma_i(\text{cm}^2) \cdot N_T, \quad (5)$$

where ϕ is the neutrino numerical flux given in Eq. (3), σ_i is the cross section of the given neutrino reaction, and N_T is the target number.

For the accelerator neutrino detection at CSNS, a detector similar to MiniBooNE [24] is adopted. It consists of a spherical 803 tons fiducial mass of mineral oil (CH_2 , density 0.845 g/cm^3) and has a fiducial radius of 6.1 m, occupying a volume of 950 m^3 . The total numbers of target protons, electrons, and ^{12}C are

$$\begin{aligned} N_T^{(p)} &= 6.90 \times 10^{31}, & N_T^{(e)} &= 2.76 \times 10^{32}, \\ N_T^{(C)} &= 3.45 \times 10^{31}. \end{aligned}$$

According to the discussions given in the previous section, the yield efficiency of $\bar{\nu}_e$ is a factor of 10^{-3} to 10^{-4} lower than that of the other neutrino species, and hence can be neglected. Then, the reaction channel of the inverse beta decay will be neglected. For the neutrino-proton elastic scattering, due to the Cerenkov energy threshold and quenching, only the high energy part of the neutrino spectra can be observed and it has always been taken to be too small in number to observe. In addition, due to the the proton structure, protons in the neutrino-proton elastic scattering are too difficult to identify and

have large systematic uncertainty [39]. Therefore, the neutrino-proton elastic scattering will be not considered in this paper.

By using the said detector at CSNS, two reaction channels will be used to detect the different species of neutrinos (ν_e , ν_μ , and $\bar{\nu}_\mu$):

(1) Neutrino-electron reactions

$$\begin{aligned} \nu_e + e^- &\rightarrow \nu_e + e^- \quad (\text{CC and NC}), \\ \nu_\mu + e^- &\rightarrow \nu_\mu + e^- \quad (\text{NC}), \\ \bar{\nu}_\mu + e^- &\rightarrow \bar{\nu}_\mu + e^- \quad (\text{NC}), \end{aligned}$$

where CC and NC stand, respectively, for the charged-current and neutral-current interactions, producing recoil electrons with energy from zero up to the kinematics maximum. The neutrino events observed through these reaction channels can be identified by the signal of the recoil electrons which are strong peaked along the neutrino direction [40, 41], and this forward peaking is usually used for experiments to distinguish the electron elastic scattering from the neutrino reactions on nuclei.

(2) Neutrino-carbon reactions

For the neutrinos and ^{12}C system, there are one charged-current and three neutral-current reactions:

Charged-current capture of ν_e :

$$\begin{aligned} \nu_e + {}^{12}C &\rightarrow {}^{12}N + e^-, \quad E_{th} = 17.34 \text{ MeV}, \\ {}^{12}N &\rightarrow {}^{12}C + e^+ + \nu_e. \end{aligned}$$

Neutral-current inelastic scattering of ν_e , ν_μ , and $\bar{\nu}_\mu$:

$$\begin{aligned} \nu_e + {}^{12}C &\rightarrow {}^{12}C^* + \nu'_e, \quad E_{th} = 15.11 \text{ MeV}, \\ \nu_\mu + {}^{12}C &\rightarrow {}^{12}C^* + \nu'_\mu, \quad E_{th} = 15.11 \text{ MeV}, \\ \bar{\nu}_\mu + {}^{12}C &\rightarrow {}^{12}C^* + \bar{\nu}'_\mu, \quad E_{th} = 15.11 \text{ MeV}, \\ {}^{12}C^* &\rightarrow {}^{12}C + \gamma. \end{aligned}$$

The charged-current events have the delayed coincidence of a β decay following the interaction. The neutral-current events have a monoenergetic γ ray at 15.11 MeV. Therefore, the charged-current and neutral-current reactions on carbon can be identified and observed by the neutrino detector [42, 43].

The effective cross sections of the above two reactions, the neutrino-electron reactions [43, 44] and neutrino-carbon reactions [45, 46], are given in Fig. 4.

The neutrino event numbers per year can be calculated using Eqs. (3) and (5). Fig. 5 shows the neutrino event numbers per year observed through two reaction channels, changing with the distance L . We found that:

(i) The event numbers per year of different species of neutrinos all decrease with the distance L for both the neutrino-electron reactions and neutrino-carbon reactions;

- (ii) The total event number of accelerator neutrinos observed through the neutrino-carbon channel is much larger than through the neutrino-electron reactions;
- (iii) For the neutrino-electron reactions, $\tilde{N}_{\nu_e}(CC+NC) > \tilde{N}_{\nu_\mu}(NC) > \tilde{N}_{\bar{\nu}_\mu}(NC)$;
- (iv) For the neutrino-carbon reactions, $\tilde{N}_{\nu_\mu}(NC) > \tilde{N}_{\bar{\nu}_\mu}(NC) > \tilde{N}_{\nu_e}(NC)$ and $\tilde{N}_{\nu_\mu}(CC+NC)$ and $\tilde{N}_{\bar{\nu}_\mu}(CC+NC)$ are both larger than $\tilde{N}_{\nu_e}(CC+NC)$.

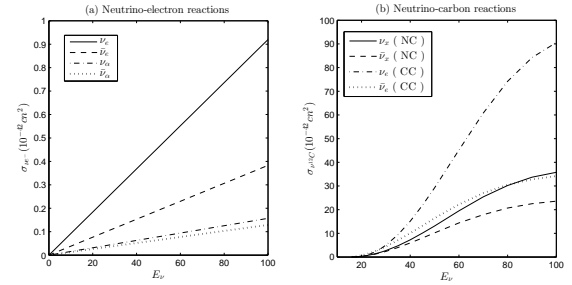


Fig. 4. The effective cross sections as functions of the neutrino energy. (a) the neutrino-electron reactions; (b) the neutrino-carbon reactions. $\alpha = \mu, \tau, x = e, \mu, \tau$.

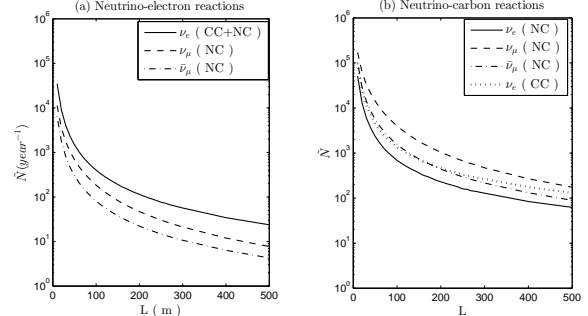


Fig. 5. The event numbers per year of accelerator neutrinos observed through various reaction channels as functions of the distance L . (a) the neutrino-electron reactions; (b) the neutrino-carbon reactions.

Table 4. Neutrino event numbers per year observed through various reaction channels for $L = 60$ m. The detector efficiency and beam-on efficiency are both taken to be 50%.

Reaction	$\tilde{N}_{\nu_e}(CC) + \tilde{N}_{\nu_e}(NC)$	$\tilde{N}_{\nu_\mu}(NC)$	$\tilde{N}_{\bar{\nu}_\mu}(NC)$
νe^-	263	123	54
$\nu^{12}C$	824 + 426	2580	1005

In the future, if the distance L , the detector efficiency, and the beam-on efficiency are defined, the neutrino event numbers per year observed through various reaction channels can be calculated accurately. For example, suppose the distance $L = 60$ m, the detector efficiency and beam-on efficiency both at 50%, the accurate

neutrino event numbers per year are given in Table 4. It is clear that there are a large number of accelerator neutrinos which can be used for measuring neutrino cross sections.

4 Summary and Discussion

In this paper, the accelerator neutrino beam has been studied in detail. With the code FLUKA, processes of accelerator neutrino production at CSNS from the proton beam on the tungsten target have been investigated, and the yield efficiency, numerical flux, average energy of different species of neutrinos have been obtained. We show that, after the complete decays of π^+ and μ^+ , three kinds of accelerator neutrinos have the same yield efficiency which is about 0.17 per proton. Therefore, they have the same yield event number per year which is 0.21×10^{22} for CSNS-I and 1.05×10^{22} for CSNS-II.

The detection of accelerator neutrinos through two reaction channels, the neutrino-electron reactions and

neutrino-carbon reactions, has been studied, and the neutrino event numbers have been calculated. It is found that the total event number of accelerator neutrinos observed through the channel of the neutrino-carbon reactions is much larger than that of the neutrino-electron reactions.

In our calculation, the detector efficiency and beam-on efficiency were not seriously considered. In the future, in the completion of the design of a neutrino detector at CSNS, the detector efficiency and beam-on efficiency will be given. Then, the detector errors will need to be reduced in the calculation of the neutrino event numbers. Furthermore, the statistical errors and systematic errors on neutrino fluxes and cross sections also need to be considered for the design of neutrino experiment.

The author would like to thank B.-L. Young, X.-H. Guo, S. Wang, and S.-J. Ding for helpful discussions and support.

References

- 1 Boardman B. Spallation Neutron Source: Description of Accelerator and Target. RL-82-006, 1982
- 2 J-PARC TDR. Accelerator Technical Design Report for High-intensity Proton Accelerator Facility Project. JAERI-Tech2003-044, 2003
- 3 SNS Project Team. Spallation Neutron Source Design Manual. June, 1998
- 4 CSNS Project Team. China Spallation Neutron Source Feasibility Reaearch Report. Institute of High Energy Physics and Institute of Physics, Chinese Academy of Sciences, 2009 (in Chinese)
- 5 ESS Central Project Team. ESS Technical Design Report. ESS-doc-274-v15, 2015
- 6 Wei J. Rev. Mod. Phys., 2003, **75**: 1383-1432
- 7 Wei J, Abell D T, Beebe-Wang et al. Phys. Rev. ST Accel. Beams, 2000, **3**: 080101
- 8 Athanassopoulos C, Auerbach L B, Bauer D et al. Nucl. Instrum. Methods Phys. Res. A, 1997, **388**: 149-172
- 9 Zeitnitz B. Prog. Part. Nucl. Phys., 1985, **13**: 445-478
- 10 Zeitnitz B. Prog. Part. Nucl. Phys., 1994, **32**: 351-373
- 11 Shirakata M J, Fujimori H, Irie Y et al. Phys. Rev. ST Accel. Beams, 2008, **11**: 064201
- 12 Saha P K, Shobuda Y, Hotchi H et al. Phys. Rev. ST Accel. Beams, 2009, **12**: 040403
- 13 SNS Project Team. Spallation Neutron Source Accumulator Ring and Transport Design Manual. June, 2003
- 14 VanDalen G J. Oscillations and Cross Sections at the SNS with a Large Cerenkov Detector. arXiv: 0309014 [nucl-ex]
- 15 Wang S, Fang S X, Fu S N et al. Chin. Phys. C, 2009, **33**: 1-3
- 16 Huang M Y, Wang S, Qiu J et al. Chin. Phys. C, 2013, **37**: 067001
- 17 Baussan E, Blennow M, Bogomilov M et al. Nucl. Phys. B, 2014, **885**: 127-149
- 18 Wei J, Fu S N, Tang J Y et al. Chin. Phys. C, 2009, **33**: 1033-1042
- 19 Kopp S E. Phys. Rep., 2007, **439**: 101-159
- 20 Burman R L, Louis W C. J. Phys. G: Nucl. Part. Phys., 2003, **29**: 2499-2512
- 21 Drexlin G, Eberhard V, Gemmeke et al. Nucl. Instrum. Methods Phys. Res. A, 1990, **289**: 490-495
- 22 Burman R L, Dodd A C, Plischke P. Nucl. Instrum. Methods Phys. Res. A, 1996, **368**: 416-424
- 23 Abe K, Abgrall N, Aihara H et al. Nucl. Instrum. Methods Phys. Res. A, 2011, **659**: 106-135
- 24 Aguilar-Arevalo A A, Anderson C E, Bartoszek L M et al. Nucl. Instrum. Methods Phys. Res. A, 2009, **599**: 28-46
- 25 Bonesini M, Guglielmi A. Phys. Rep., 2006, **433**: 65-126
- 26 Bulanov S V, Esirkepov T, Migliozzi P et al. Nucl. Instrum. Methods Phys. Res. A, 2005, **540**: 25-41
- 27 Lazauskas R, Volpe C. J. Phys. G: Nucl. Part. Phys., 2010, **37**: 125101
- 28 Louis W C. Prog. Part. Nucl. Phys., 2009, **63**: 51-73
- 29 Aguilar-Arevalo A A, Bazarko A O, Brice S J et al. Phys. Rev. Lett., 2007, **98**: 231801
- 30 Gervey G T, Green A, Green C et al. Phys. Rev. D, 2005, **72**: 092001
- 31 Ferrari A, Sala P R, Fasso A et al. Fluka: Multi-Particle Transport Code. CERN-2005-010, 2011
- 32 Vergados J D, Avignone III F T, Giomataris I. Phys. Rev. D, 2009, **79**: 113001
- 33 Olive K A, Agashe K, Amsler C et al. Chin. Phys. C, 2014, **38**: 090001
- 34 Huang M Y, Guo X H, Young B L. Phys. Rev. D, 2010, **82**: 033011
- 35 Xu J, Huang M Y, Hu L J et al. Commun. Theor. Phys., 2014, **61**: 226-234
- 36 Dore U, Orestano D. Rep. Prog. Phys., 2008, **71**: 106201
- 37 Gapozzi F, Fogli G L, Lisi E et al. Phys. Rev. D, 2014, **89**:

093018

38 Elnimr M, Stancu I, Yeh M et al. The OscSNS White Paper. arXiv:1307.7097 [physics.ins-det]

39 Beacom J F, Palomares-Ruiz S. Phys. Rev. D, 2003, **67**: 093001

40 Allen R C, Chen H H, Doe P J et al. Phys. Rev. D, 1993, **47**: 11-28

41 Imlay R, VanDalen G J. J. Phys. G: Nucl. Part. Phys., 2003, **29**: 2647-2664

42 Auerbach L B, Burman R L, Caldwell D O et al. Phys. Rev. C, 2002, **66**: 015501

43 Cadonati L, Calaprice F P, Chen M C. Astropart. Phys., 2002, **16**: 361-372

44 Arafuno J, Fukugita M. Phys. Rev. Lett., 1987, **59**: 367-369

45 Fukugita M, Kohyama Y, Kubodera K. Phys Lett. B, 1988, **212**: 139-144

46 Kolbe E, Langanke K, Vogel P. Nucl. Phys. A, 1999, **652**: 91-100